Chinese Chemical Letters 35 (2024) 108655

Contents lists available at ScienceDirect

Chinese Chemical Letters

journal homepage: www.elsevier.com/locate/cclet

Enhanced electrochemical performance of nanoscale single crystal NMC811 modification by coating $LiNbO_3$

Fengyu Zhang[a,b], Yali Liang[a], Zhangran Ye[a], Lei Deng[a], Yunna Guo[a], Ping Qiu[b], Peng Jia[a,c,*], Qiaobao Zhang[d,*], Liqiang Zhang[a,*]

[a] Clean Nano Energy Center State Key Laboratory of Metastable Materials Science and Technology, Yanshan University, Qinhuangdao 066004, China
[b] School of New Energy and Materials, China University of Petroleum Beijing, Beijing 102249, China
[c] Hebei Key Laboratory of Applied Chemistry, College of Environmental and Chemical Engineering, Yanshan University, Qinhuangdao 066004, China
[d] State Key Laboratory of Physical Chemistry of Solid Surfaces, College of Materials, Xiamen University, Xiamen 361005, China

ARTICLE INFO

Article history:
Received 8 April 2023
Revised 24 May 2023
Accepted 5 June 2023
Available online 9 June 2023

Keywords:
Ni-rich NMC811
Molten salt method
Nanonization
Surface coating
Micron cracks

ABSTRACT

Single crystallization is an important strategy to resolve intergranular cracks and unnecessary side reactions with electrolytes in layered transition metal oxide cathodes $LiNi_{0.8}Mn_{0.1}Co_{0.1}O_2$ (NMC811). Due to the limitations of high-temperature sintering and multi-step calcination, single crystal NMC811 generally shows irregular particles with a size of 2–3 μm. However, the prolonged Li-ion diffusion pathway and the stress generated by the uneven de-/intercalation sluggish Li-ion diffusion kinetics, what is more, cause structural damage such as intragranular cracks. A slow Li extraction rate or particle size reduction will ameliorate the structural damage and improve the cycling stability. As the most promising cathodes for next-generation power batteries, NMC811 required fast charge performance and cycle stability. Particle size reduction appears to be the displacement option. Nanonization is an effective strategy to mitigate intragranular cracks of single crystal NMC811. However, the serious aggregation and increased specific surface area become new challenges. In this article, we synthesized monodisperse nanoscale single crystal NMC811 by molten salt method and modified the surface by $LiNbO_3$ coating. The electrochemical performance shows that nanoscale single crystal NMC811 has faster kinetic and higher capacity retention, so the strategy of combining nanonization and surface coating is an alternative way to prepare high specific capacity and cycle stable single crystal NMC811.

Transition metal layered oxide cathodes ($LiNi_xMn_yCo_{1-x-y}O_2$, NMCs) are promising cathode materials for electric vehicle Li-ion batteries due to their high energy density and suitable cost [1–4]. Improving the energy density, cycle life, and fast charging performance of Li-ion batteries has always been the focus of researches [5,6]. As an important component of Li-ion batteries, increasing the nickel content in NMCs is an important strategy to improve energy density, although this brings new challenges [7,8]. The structural stability and cycle life of Ni-rich NMCs deteriorate due to enhanced cation mixing and sudden lattice collapse, which can lead to intergranular cracks, especially for typical polycrystalline secondary particles [9–11]. The newly generated intergranular cracks will expose fresh surfaces and cause unwanted side reactions with the electrolyte [12,13]. Although various designs such as doping and surface coating have been proposed, it is difficult to completely suppress such intergranular cracks [14–17]. Single crystal NMC is considered to be an effective solution against intergranular cracks due to the absence of grain boundaries [18,19].

Single crystal NMC811 is generally synthesized by high-temperature sintering and multi-step calcination, and high temperature promotes ion diffusion, resulting in a single crystal particle size of 2–3 μm. The studies have shown that prolonged Li-ion diffusion pathway and the stress generated by the uneven de-/intercalation sluggish Li-ion diffusion kinetics and cause intragranular cracks [20,21]. Ryu *et al.* [22] revealed the spatially inhomogeneous lithium concentrations in single crystal NMC cathode during cycling. This phenomenon is exacerbated by fast de-/intercalation and Ni contents. Slow Li-ion diffusion and reduced grain size may be effective ways to relieve internal stress. However, for power batteries that require rate performance, it may be necessary to reduce the grain size of single crystal NMC811.

The synthesis of single crystal NMC811 have challenges due to the relatively low lithiation temperature and intensified cation mixing at high temperatures [23,24]. Therefore, molten salt

* Corresponding authors.
E-mail addresses: pengjia@ysu.edu.cn (P. Jia), zhangqiaobao@xmu.edu.cn (Q. Zhang), lqzhang@ysu.edu.cn (L. Zhang).

https://doi.org/10.1016/j.cclet.2023.108655
1001-8417/

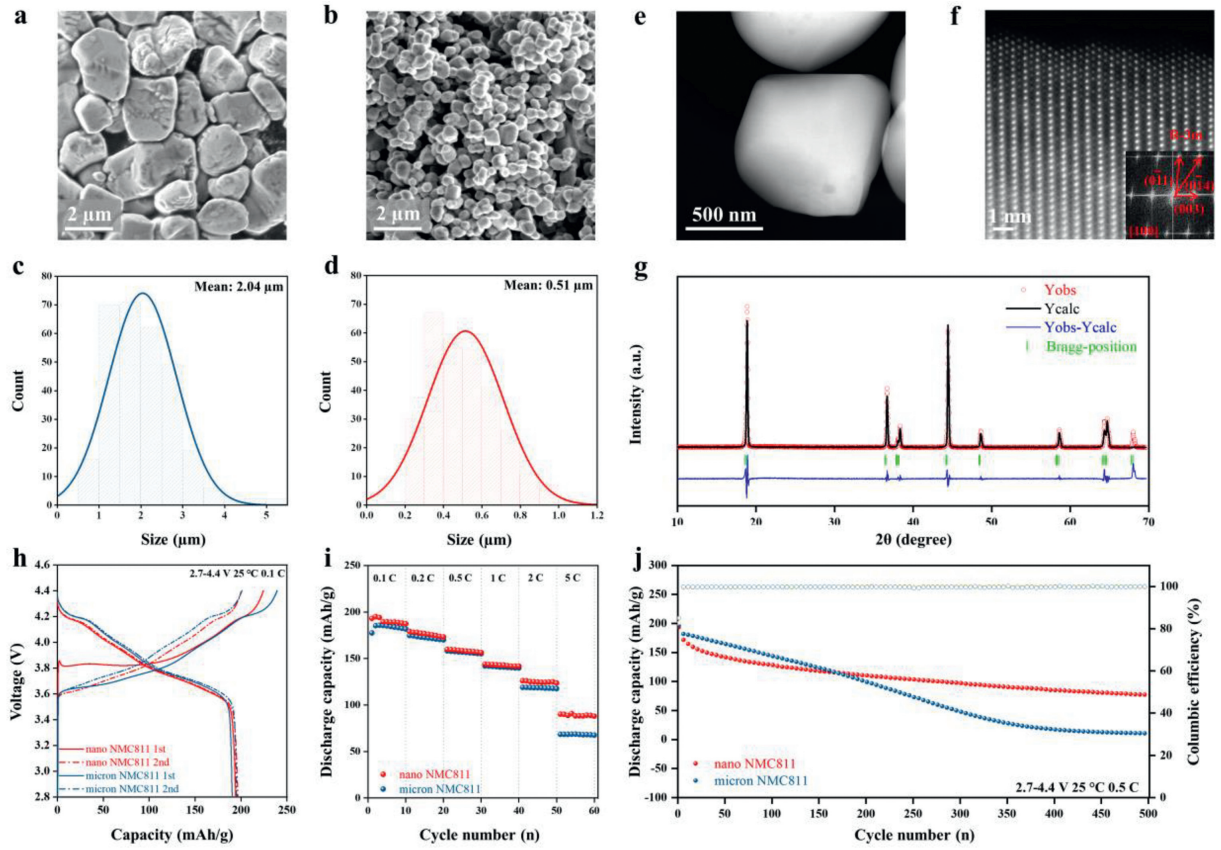

Fig. 1. SEM image of (a) micron NMC811 and (b) nano NMC811. Single crystal particle size distribution of (c) micron NMC811 and (d) nano NMC811. (e) STEM image of nano NMC811. (f) High angle annular dark field (HAADF) image and corresponding fast Fourier transform (FFT) of nano NMC811. (g) XRD pattern of nano NMC811. (h) Charge/discharge profile at 0.1 C, (i) rate performance and (j) discharge capacity and Coulombic efficiency during cycling at 0.5 C of nano NMC811 and micron NMC811.

method is considered as an alternative method, and grains with different morphologies and exposed crystal planes can be prepared by adjusting process parameters [25,26]. Due to the separation from the O_2 atmosphere caused by the solution properties of the molten salt, most studies focus on NMC111 and NMC532 [27,28]. When the molten salt composition contains a large amount of nitrate with oxidizing properties, Ni-rich NMC811 is successfully synthesized. Guo *et al.* [29] synthesized micron scale single crystal $LiNi_{0.8}Mn_{0.1}Co_{0.1}O_2$ using a mixture of $LiNO_3$ and LiOH as molten salt. Due to the low melting point of nitrate, the synthesized single crystal NMC811 is usually micron in size, which may cause structural damage at the end of charging. Zhang *et al.* [30] studied the close relationship between surface structure, internal stress and capacity fading. The pristine surface chemistry, concomitant phase heterogeneity, and induced stress deteriorate structural integrity along with cycling performance. Surface chemical regulation can induce uniform phase distribution in single crystals, helping to improve surface chemical stability and performance retention [31]. Fan *et al.* [32] reported a strategy to construct an *in situ* $Li_{1.4}Y_{0.4}Ti_{1.6}(PO_4)_3$ ion/electron conductive network which interconnects single crystal Ni-rich NMC particles. This strategy facilitates the Li-ion transport between single crystal NMC particles, mitigates mechanical instability and prevents detrimental crystalline phase transformation. Therefore, reducing particle size and modifying surface of single crystal NMC811 are effective strategy to alleviate structural damage and improve stability. In solid-state batteries with non-wetting electrolytes, nanoscale cathodes are theoretically more advantageous than micron scale polycrystalline and single crystal cathodes because of structural integrity and smaller volume changes during cycling [33–36].

In this article, we synthesis nanoscale single crystal NMC811 using molten salt method and modified its surface structure by coating $LiNbO_3$. Compared with commercial micron scale single crystal NMC811, the optimized nano NMC811 has better Li-ion diffusion kinetics and structural stability. Our work provides a new insight for improved design of Ni-rich NMC811 in the field of electric vehicles with high energy density, long cycle life and fast charging performance.

We prepared nanoscale single crystal NMC811 using mixed molten salts of Na_2SO_4, LiOH and $LiNO_3$. The characterization of its morphology and structure is shown in Fig. 1. It can be seen from the SEM image that the prepared nano NMC811 is monodispersed. By counting more than 300 particles, we obtained the particle size distribution map of nano NMC811 and micron NMC811 (Figs. 1c and d). The particle size of nano NMC811 presents a normal distribution and about 510 nm in size, while the micron NMC811 shows 2.04 μm in size. The XRD patterns for the as prepared nano NMC811 and micron NMC811 are shown in Fig. 1g and Fig. S1 (Supporting information), which can be indexed to the α-$NaFeO_2$ hexagonal structure corresponding to a R-3m space group, without any additional peak. Further, the peak intensity ratio $I_{(003)}/I_{(104)}$ of nano NMC811 is obvious lower than the micron NMC811, which indicates more cation mixing due to the loss of Li-ions during the water washing process when removing molten salt. The microstructure of nano NMC811 is characterized by scanning transmission electron microscopy (STEM) as shown in Figs. 1e and f. There has a small amount of nanopores in the bulk and a 3 nm thick cation mixing zone on the surface. The electrochemical performance of the nano NMC811 and micron NMC811 were tested using a CR2032 coin type half-cell with lithium metal as

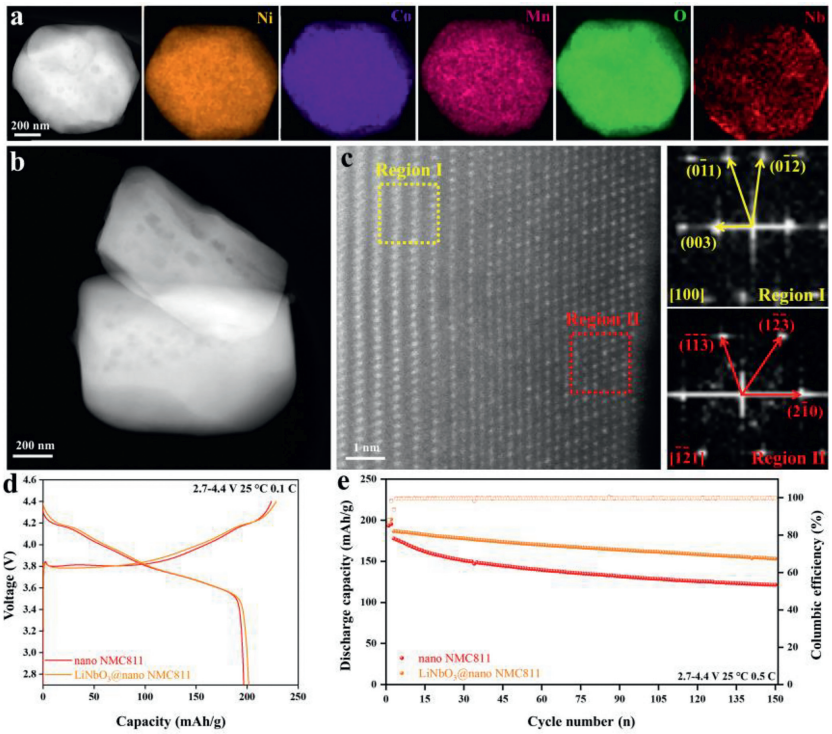

Fig. 2. (a) Elements mapping of $LiNbO_3$@nano NMC811. (b) STEM image of $LiNbO_3$@nano NMC811. (c) HAADF image and corresponding FFT of $LiNbO_3$@nano NMC811. (d) Charge/discharge profile at 0.1 C, (e) discharge capacity and Coulombic efficiency during cycling at 0.5 C of nano NMC811 and $LiNbO_3$@nano NMC811.

the counter electrode. Fig. 1h shows first and second cycle charge and discharge curves at 0.1 C between 2.7 V and 4.4 V. The charging voltage of nano NMC811 is above 3.8 V in the first cycle, and then reduced to 3.6 V in the second cycle, which is related to the lithium-poor area on the surface. The high initial charge voltage reflects the difficulty of Li^+ extraction. Since nano NMC811 is prepared by the molten salt method, the lithium-poor layer remains on the particle surface during the process of removing the molten salt, so it is difficult for Li^+ (inside the particles) to be extracted. During the second charge process, the Li^+ concentration in the surface lithium-poor region was improved, so the initial charge voltage was reduced to 3.6 V. The nano NMC811 and micron NMC811 deliver an initial discharge capacity of 194.5 and 190.6 mAh/g, an initial Columbic efficiency of 86.7% and 79.6%, respectively. In the second cycle, the discharge specific capacity and Coulombic efficiency of nano NMC811 and micron NMC811 are similar, which is due to the intensification of surface side reactions caused by nanonization. This phenomenon also occurs in rate performance and stability test (Figs. 1i and j). In the early of charge and discharge, nano NMC811 has a sharp decay of capacity, resulting in unsatisfactory rate performance and discharge specific capacity. However, after 500 cycles at 0.5 C, the capacity retention of nano NMC811 is 39.9%, while that of micron NMC811 is 5.3%. Micron NMC811 suffered structural damage in the end of charge, resulting in a continuous decline in capacity, while nano NMC811 only consumed electrolyte in the early of cycles. CV curves of nano and micron NMC811 from the 1^{st} to 3^{rd} cycle with a sweep rate of 0.1 mV/s (Fig. S2 in Supporting information). It can be seen that the redox peaks of cathode began to weak and deviation, indicating a worse polarization of nano NMC811. The Nyquist curves, obtained by fitting in the equivalent circuit, are composed of a semicircle in the high-frequency region, a semicircle in the intermediate region, and a straight line in the low-frequency region, representing membrane impedance (R_{sf}), charge transfer impedance (R_{ct}), and Warburg impandance (W_o), respectively [37,38]. After 100 cycles at 1 C, the impedance of the nano NMC811 increases from 253.1 Ω to 380.5 Ω, while that of the micron NMC811 decreases from 304.9 Ω to 67.3 Ω (Fig. S3 in Supporting information). The initial impedance of the nano NMC811 is low, and after electrolyte infiltration and electrochemical reaction, its impedance is much larger than that of the micron NMC811. The results show that the nano NMC811 has more cathode electrolyte interfacial layer (CEI) than the micron NMC811 due to nanonization. Therefore, mitigating the side reaction with electrolyte is of great significance to improve the capacity and stability of nano NMC811.

Surface coating is an effective method to alleviate the side reaction between active materials and electrolyte. We coated the surface of nano NMC811 and micron NMC811 with $LiNbO_3$, respectively. The elements distribution mapping after surface modification is shown in Fig. 2a and Fig. S4 (Supporting information). It can be seen that the expected elements are evenly distributed, and Nb element is concentrated on the surface. We characterized the microstructure of $LiNbO_3$@nano NMC811 using STEM. $LiNbO_3$@nano NMC811 is shown as irregular particles with a particle size of about 500 nm, and a small amount of nanopores inside (Fig. 2b). The HAADF image and the corresponding FFT show that its surface is a biphasic structure, and the region I and region II correspond to NMC811 and $LiNbO_3$, respectively (Fig. 2c). After coating modification, the initial discharge specific capacity of $LiNbO_3$@nano NMC811 increased to 201.6 mAh/g, and the stability also increased from 62.7% to 76.5% after 150 cycles at 0.5 C (Figs. 2d and e). The stability of $LiNbO_3$@micron NMC811 is also improved in Fig. S5 (Supporting information). This indicates that the surface coating of $LiNbO_3$ increases the Li-ion diffusion channel and prevents the side reaction of the active material with the electrolyte.

After being coated with $LiNbO_3$ on the surface, the electrochemical performance of nano NMC811 is significantly better than that of micron NMC811. As shown in Fig. 3a, $LiNbO_3$@nano NMC811 has higher initial discharge specific capacity and Coulombic efficiency, which may be due to the special crystal face of

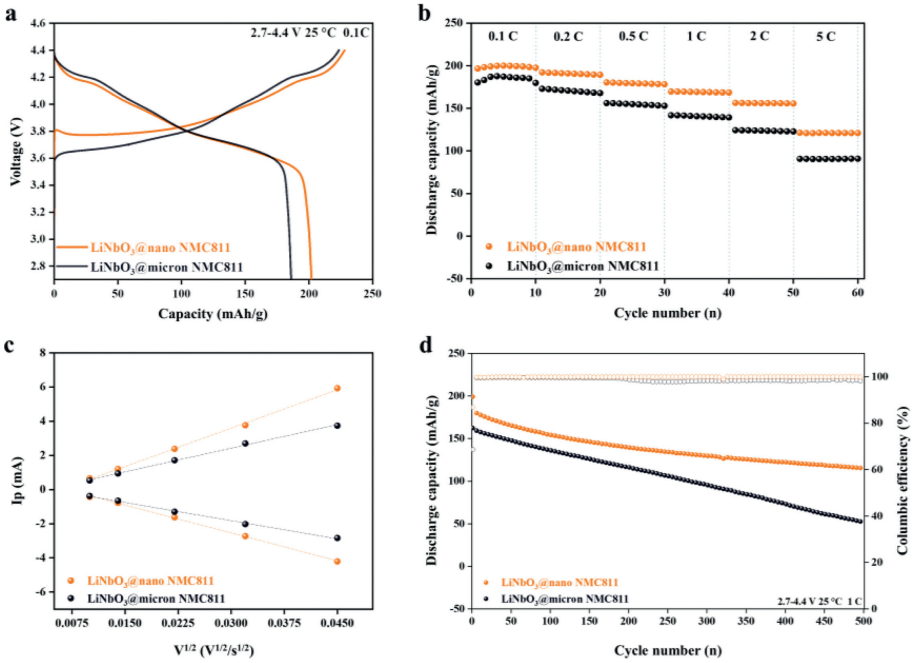

Fig. 3. Electrochemical performance comparison of $LiNbO_3$@nano NMC811 and $LiNbO_3$@micron NMC811. (a) Charge/discharge profile at 0.1 C, (b) rate performance, (c) apparent diffusion coefficient, (d) discharge capacity and Coulombic efficiency during cycling at 1 C of $LiNbO_3$@nano NMC811 and $LiNbO_3$@micron NMC811.

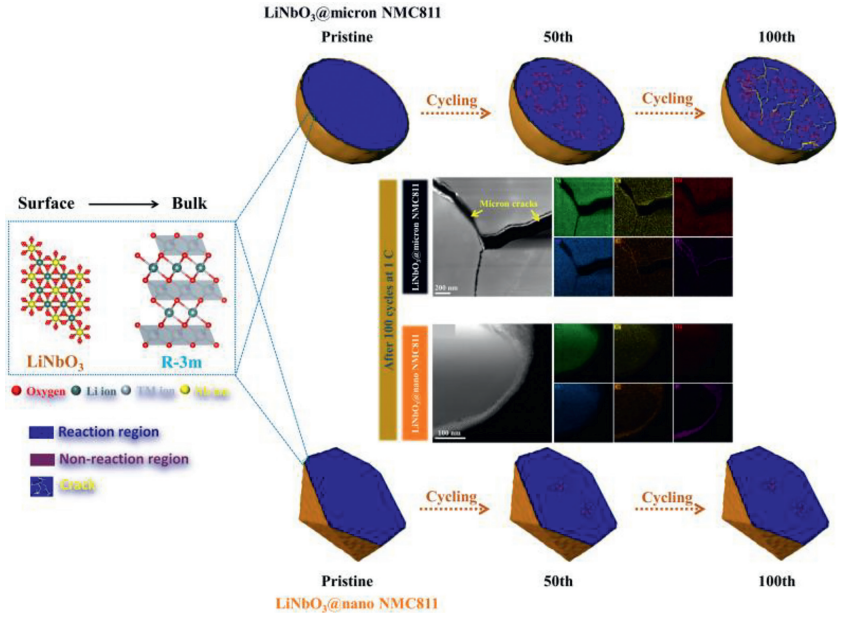

Fig. 4. Schematic diagram of the failure mechanism of $LiNbO_3$@nano NMC811 and $LiNbO_3$@micron NMC811.

nano NMC811 prepared by molten salt method, and the coating of $LiNbO_3$ increases the diffusion of lithium ions. However, for micron NCM811 spherical particles prepared by high-temperature solid-state sintering method, coating $LiNbO_3$ has little effect on its initial discharge specific capacity. Otherwise, the initial charge voltage of the $LiNbO_3$@nano NMC811 can reach 3.8 V, far exceeding the voltage of the $LiNbO_3$@micron NMC811 at 3.6 V, which is due to the presence of a lithium-poor layer on the surface of nano particles. The rate performance was evaluated at various rates ranging from 0.1 C to 5 C (Fig. 3b). The $LiNbO_3$@nano NMC811 delivers a higher reversible capacity comparable to the $LiNbO_3$@micron NMC811 at the same current. Even at a rate of 1 C, the $LiNbO_3$@nano NMC811 delivers a reversible capacity of 169.7 mAh/g (86.3% of the capacity at 0.1 C), higher than 141.8 mAh/g of micron NMC811 (78.6% of the capacity at 0.1 C). We tested the CV curve at various scan rate from 0.1 mV/s to 2 mV/s (Fig. S6 in Supporting information). Fig. 3c shows a clearly liner relationship between peak current and scan rate, indicating diffusion-controlled behavior. The slope of the liner indicated that Li-ion diffusion of $LiNbO_3$@nano NMC811 is larger than $LiNbO_3$@micron NMC811 at charge and discharge process. This proves to be a significant advantage in using a $LiNbO_3$@nano NMC811 as a cathode material. During the long-term cycling at 1 C, the $LiNbO_3$@nano NMC811 maintains a capacity of 115.6 mAh/g after 500 cycles when cycled in the voltage rang of 2.7–4.4 V, while the $LiNbO_3$@micron NMC811 has a capacity of 52.3 mAh/g applying the same measurement protocol (Fig. 3d).

The Li-ion diffusion pathway of nano NCM811 is reduced, which alleviates the microcracks caused by uneven de/intercalation and stress (Fig. 4 and Fig. S7 in Supporting information). Microcracks expose new reaction sites, consume electrolyte, and increase transition metal dissolution. The surface coating modification further reduces the side reaction with the electrolyte. It can be seen from the CV curves that after 100 cycles with a current density of 1 C, the polarization of nano NMC811 has been greatly reduced (Fig. S8 in Supporting information). As shown in Fig. S9 (Supporting information), the impedance is also much lower than that of uncoated, almost similar to that of micron NMC811.

In summary, we prepared nanoscale single crystal NMC811 using the molten salt method. Although the specific capacity and stability are improved, the increased specific surface area of the nanonization leads to serious side reactions with the electrolyte. Surface modification with $LiNbO_3$ isolates NMC811 active material and electrolyte, and increases Li-ion diffusion channels. Compared with commercial $LiNbO_3$@micron NMC811, nanonized NMC811 has better electrochemical performance. This suggests that the nanonization of single crystal NMC811 with $LiNbO_3$ modification layer represents a promising strategy for high power applications in LIBs.

Declaration of competing interest

The authors declare that they have no know competing financial interests or personal relationships that could have appeared to influence the work reported in this paper.

Acknowledgments

This work was financially supported by the National Natural Science Foundation of China (Nos. 52022088, 51971245, 51772262, U20A20336, 21935009), Natural Science Foundation of Hebei Province (Nos. F2021203097, B2020203037). China Postdoctoral Science Foundation (No. 2021M702756).

Supplementary materials

Supplementary material associated with this article can be found, in the online version, at doi:10.1016/j.cclet.2023.108655.

References

[1] Y. Ding, Z.P. Cano, A. Yu, J. Lu, Z. Chen, Electrochem. Energy Rev. 2 (2019) 1–28.
[2] Y. Tian, G. Zeng, A. Rutt, et al., Chem. Rev. 121 (2020) 1623–1669.
[3] Y. Na, X. Sun, A. Fan, S. Cai, C. Zheng, Chin. Chem. Lett. 32 (2021) 973–982.
[4] S. Yang, B. Wang, Q. Lv, et al., Chin. Chem. Lett. 34 (2023) 107783.
[5] B.P. Thapaliya, S. Misra, S.Z. Yang, et al., Adv. Mater. Interfaces 9 (2022) 2200035.
[6] C. Mao, R.E. Ruther, J. Li, Z. Du, I. Belharouak, Electrochem. Commun. 97 (2018) 37–41.
[7] C.D. Quilty, P.J. West, G.P. Wheeler, et al., J. Electrochem. Soc. 169 (2022) 020545.
[8] T.M. Heenan, A. Wade, C. Tan, et al., Adv. Energy Mater. 10 (2020) 2002655.
[9] Y. Gao, J. Park, X. Liang, ACS Appl. Energy Mater. 3 (2020) 8978–8987.
[10] K. Taghikhani, P.J. Weddle, J. Berger, R.J. Kee, J. Electrochem. Soc. 168 (2021) 080511.
[11] Y. Su, Q. Zhang, L. Chen, et al., J. Energy Chem. 65 (2022) 236–253.
[12] W. Xue, M. Huang, Y. Li, et al., Nat. Energy 6 (2021) 495–505.
[13] M. Yoon, Y. Dong, J. Hwang, et al., Nat. Energy 6 (2021) 362–371.
[14] Y.G. Zou, H. Mao, X.H. Meng, et al., Angew. Chem. Int. Ed. 60 (2021) 26535–26539.
[15] C. Zhang, J. Wan, Y. Li, et al., J. Mater. Chem. A 8 (2020) 6893–6901.
[16] T. Watanabe, T. Yokokawa, M. Yamada, et al., RSC Adv. 11 (2021) 37150–37161.
[17] H. Wang, Y. Chu, Q. Pan, et al., Electrochim. Acta 366 (2021) 137476.
[18] H. Zhu, Y. Tang, K.M. Wiaderek, et al., Nano Lett. 21 (2021) 9997–10005.
[19] Q. Guo, J. Huang, Z. Liang, et al., New J. Chem. 45 (2021) 3652–3659.
[20] Y. Bi, J. Tao, Y. Wu, et al., Science 370 (2020) 1313–1317.
[21] G.M. Han, Y.S. Kim, H.H. Ryu, Y.K. Sun, C.S. Yoon, ACS Energy Lett. 7 (2022) 2919–2926.
[22] H.H. Ryu, B. Namkoong, J.H. Kim, et al., ACS Energy Lett. 6 (2021) 2726–2734.
[23] J.H. Shim, C.Y. Kim, S.W. Cho, et al., Electrochim. Acta 138 (2014) 15–21.
[24] X. Li, K. Zhang, S. Wang, et al., Sustain. Energy Fuels 2 (2018) 1772–1780.
[25] Z. Qin, Z. Wen, Y. Xu, et al., Small 18 (2022) e2106719.
[26] X. Chen, Y. Feng, S. Zhang, et al., J. Alloys Compd. 900 (2022) 163308.
[27] T. Kimijima, N. Zettsu, K. Teshima, Cryst. Growth Design 16 (2016) 2618–2623.
[28] T. Kimijima, N. Zettsu, K. Yubuta, et al., J. Mater. Chem. A 4 (2016) 7289–7296.
[29] Z. Guo, Z. Jian, S. Zhang, et al., J. Alloys Compd. 882 (2021) 160642.
[30] F. Zhang, S. Lou, S. Li, et al., Nat. Commu. 11 (2020) 3050.
[31] X. Fan, Y. Huang, H. Wei, et al., Adv. Funct. Mater. 32 (2022) 2109421.
[32] X. Fan, X. Ou, W. Zhao, et al., Nat. Commun. 12 (2021) 5320.
[33] Y. Han, S.H. Jung, H. Kwak, et al., Adv. Energy Mater. 11 (2021) 2100126.
[34] E. Trevisanello, R. Ruess, G. Conforto, F.H. Richter, J. Janek, Adv. Energy Mater. 11 (2021) 2003400.
[35] S. Sun, C.Z. Zhao, H. Yuan, et al., Mater. Futures 1 (2022) 012101.
[36] S. Sun, C.Z. Zhao, H. Yuan, et al., Sci. Adv. 8 (2022) eadd5189.
[37] L. Liang, X. Li, M. Su, et al., Angew. Chem. Int. Ed. 62 (2023) e202216155.
[38] L.F. Wang, M.M. Geng, X.N. Ding, et al., Met. Mater. 28 (2021) 538–552.